Fire Whirls

Ali Tohidi[1], Michael J. Gollner[1], and Huahua Xiao[2]

[1]Department of Fire Protection Engineering, University of Maryland, College Park, MD, USA, 20740; email: mgollner@umd.edu
[2]Department of Aerospace Engineering, University of Maryland, College Park, MD, USA, 20740

Annual Review of Fluid Mechanics 2018. 50:1–28

This article's doi: 10.1146/annurev-fluid-122316-045209

Keywords

Fire Whirl, Tornado, Vortex, Combustion, Vortex Breakdown

Abstract

Fire whirls have long fascinated the research community, however their destructive power has hidden many features of their formation, growth and propagation. Most of what is known about fire whirls, therefore, comes from scale modeling experiments in the laboratory. Both the methods of formation, dominated by wind and geometry, and the inner structure of the whirl, including velocity and temperature fields, have been studied at this scale. The particular case of quasi-steady fire whirls directly over a fuel source forms the bulk of current experimental knowledge, despite many other cases existing in nature. The present article reviews the state of knowledge concerning the fluid dynamics of fire whirls, including the conditions for their formation, their structure and the mechanisms which control their unique state. Finally, recent discoveries will be highlighted as well as potential research avenues for the future.

Contents

1. INTRODUCTION

The fire whirl is one of the most dramatic structures which arises at the intersection of combustion and fluid mechanics. Throughout the literature, fire whirls have been identified by a variety of names such as devil, tornado, twister, whirlwind, or even dragon twist (Japanese). Regardless of the name, when the right combination of wind and fire interact, the result is an intensification of combustion with whirling flames which we call the fire whirl. While the fire whirl or "fire tornado" shares some features with its atmospheric counterparts, it remains distinct in its source of buoyancy, combusting fuel, structure, and formation patterns. In nature, fire whirls are most often observed in mass fires. These include both large wildland (also known as forest or bush fires) and urban conflagrations such as the burning of cities or towns. Due to the diversity of topography, wind, and fire conditions that can occur in wildland fires, fire whirls are a frequent phenomenon. Figure 1 shows a multitude of conditions under which various types of fire whirls are formed. Fire whirls have mostly been studied in the context of fire safety, as their erratic movement and ability to loft burning firebrands contribute to the rapid ignition of new fires, presenting significant hazards to nearby firefighting personnel (Countryman 1971; Forthofer and Goodrick 2011).

Despite the incredible interest they can garner, fire whirls remain a relatively poorly understood phenomenon due to their convoluted dynamics and difficulties in obtaining quantitative data (Soma and Saito 1991; Albini 1984; Morton 1970). Hence, many details of the fire whirl, whether formed in the laboratory or by natural means, remain elusive. This article will review the literature on fire whirls, beginning with description of important parameters governing their dynamics followed by review of the various formation mechanisms and a detailed description of the inner structure of the fire whirl. Finally, the processes governing the fire whirl will be reviewed along with concluding remarks and avenues for future research.

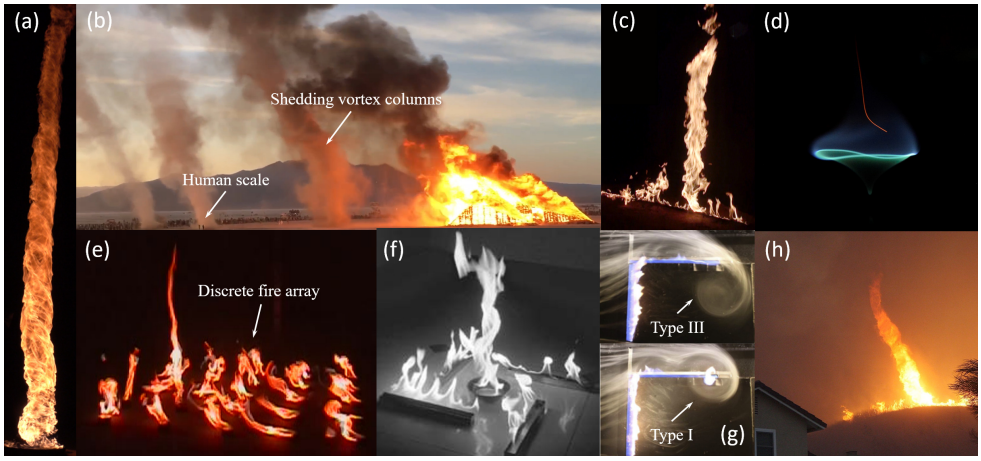

Figure 1

Shown are various forms and scales of fire whirls; (a) Full structure of a 30 cm diameter pool Heptane fire whirl in the laboratory at the University of Maryland, (b) Shedding columns of whirling hot gases in the wake of a fire plume during the "Burning Man" event (courtesy of Jeff Kravitz), (c) Formation of a fire whirl over a line burner with cross-flow (Zhou et al. 2016), (d) the blue whirl, thought to form due to vortex breakdown (Xiao et al. 2016), (e) Formation of a fire whirl due to interaction of multiple fire sources with cross-flow (Liu et al. 2007), (f) Fire whirl formation from multiple fires without wind (Zhou and Wu 2007), (g) Generation of whirling columns of hot gases over an L-shaped fire source with 1 cm width through a 0.2 m/s cross-flow (Kuwana et al. 2013), (h) an inclined fire whirl at the wildland-urban interface during the Freeway Complex fire in Yorba Linda, California, November 2008 (David McNew, GETTY IMAGES).

2. INFLUENTIAL PARAMETERS

Due to fire whirls high intensity, laboratory-scale experiments have primarily been used to model these destructive forces of nature. Much knowledge can be gained by examining the governing equations of mass, momentum and energy, and conducting dimensional analysis on the parameter space. These influential parameters can be summarized as

$$(U_r, U_z, \Gamma, H, \dot{m}) = \Phi\left(L_h, \dot{\mathcal{Q}}, C_p, \Delta\rho, \rho, \Delta T, T, g, \mu, \beta, \kappa, D_s\right), \tag{2.1}$$

where $\mathbf{U} = (U_r, U_\theta, U_z)$ is the time-averaged velocity vector with radial, azimuthal, and axial components in the cylindrical coordinate system, i.e. $(r, \theta, z) \in \mathbb{R}^3$. This coordinate system, with its origin set at the height of the radial boundary layer thickness above the fuel source and its z axis aligned with the (vertical) fire whirl's axis of symmetry, serves as the inertial frame of reference. $\Gamma = \oint_{\mathcal{C}} \mathbf{U} \cdot d\mathbf{l} = 2\pi r U_\theta$ denotes circulation, H is the flame height, $\dot{m}$ is the total mass-loss (burning) rate of the fuel, $\dot{\mathcal{Q}}$ is the heat-release rate, C_p denotes specific heat capacity, ρ is density, and T is temperature. The density difference and excess temperature are represented by $\Delta\rho$ and ΔT, respectively. Also, g represents acceleration due to gravity, μ is the dynamic viscosity of the gas, β is the coefficient of thermal expansion of the gas, κ the thermal conductivity of the gas, D_s is the molecular diffusion coefficient of species, and L_h denotes a characteristic horizontal length scale. The choice of L_h varies throughout the literature and is often replaced by D_0, which is the pool or burner diameter (Thomas 1963; Emmons and Ying 1967; Soma and Saito 1988; Kuwana et al. 2008; Chow et al. 2010; Lei et al. 2011; Zhou et al. 2011; Lei et al. 2012; Zhou et al.

2013), or the horizontal length scale of an obstruction (Kuwana et al. 2007). Alternatively, the diameter of the whirl, i.e. $D_w = 2b_w$, or the spacing/gap size in various experimental configurations are used for L_h in certain studies (Hartl and Smits 2016; Hartl 2016).

Applying Buckingham-Π theorem to the parameter space leads to the development of thirteen non-dimensional groups,

$$\Pi_1 = \frac{U_z}{\sqrt{gH}}, \Pi_2 = \frac{\rho\Gamma}{\mu}, \Pi_3 = \frac{H}{L_h}, \Pi_4 = \frac{\dot{m}}{\rho\sqrt{gL_h^5}}, \Pi_5 = \frac{U_r L_h}{\Gamma}, \Pi_6 = \frac{\dot{\mathcal{Q}}}{\rho C_p \Delta T U_z L_h^2}, \Pi_7 = \frac{C_p \mu}{\kappa},$$
$$\Pi_8 = \Delta\rho/\rho, \Pi_9 = \Delta T/T, \Pi_{10} = \beta\Delta T, \Pi_{11} = \frac{g\rho^2 L_h^3}{\mu^2}, \Pi_{12} = \frac{U_r}{U_z}, \Pi_{13} = \frac{\rho L_h D_s}{\dot{m}}. \tag{2.2}$$

Π_1 denotes the Froude number (Fr), based on the axial velocity component and can be used to indicate the role of buoyancy in flame structure or formation (Emori and Saito 1982; Grishin et al. 2005; Akhmetov et al. 2007; Kuwana et al. 2007, 2008). Π_2 is the (vortex core) Reynolds number based on the azimuthal velocity component (Mullen and Maxworthy 1977), and Π_7 is the flow's Prandtl number. Other non-dimensional parameters can be derived using these groups. For instance, the Rossby number, the ratio of nonlinear acceleration to Coriolis acceleration due to rotation, can be obtained from $Ro = (\Pi_3 \times \Pi_5)/\Pi_{12} = U_z H/\Gamma$. Ro can be interpreted to determine critical conditions under which a fire whirl could form (Emmons and Ying 1967; Grishin 2007), and it has been reported that in geostrophic flow with strong circulation (low Ro) the swirling behavior can be described better by Ro rather than Fr (Chuah et al. 2011). It should be noted that the Coriolis force is almost always neglected as the size of fire whirls are too small compared to the Earth's radius to be significant (Morton 1970; Lei et al. 2015a). Also, the similarity criterion may vary by orders of magnitude for vortices of different scales (Akhmetov et al. 2007). Therefore, the Grashof number, $Gr = \Pi_{10} \times \Pi_{11} = (g\beta\Delta T L_h^3)/\nu^2$ in which $\nu = \mu/\rho$, or the Reynolds number may be employed to quantify the similarity. Having obtained Re, Gr, and Pr, the Richardson and Rayleigh numbers can also be defined as $Ri = Gr/Re^2$ and $Ra = Gr \times Pr$, respectively. In this context, the Richardson number is the ratio of centrifugal forces in a density stratified field to shear forces, and Ro is conversely proportional to the swirl number provided that the vortex core pressure difference with ambient is neglected (Beér and Chigier 1972). However, there are two different mechanisms involved in damping turbulence in fire whirls: a cyclostropic force balance and radial density stratification. Accordingly, Lei et al. (2015b) introduces two simpler definitions of Ri in order to discuss turbulence suppression. This shall be discussed in more detail in section 5.3. Two other important parameters can be derived from Π-groups introduced in 2.2. First, $\dot{\mathcal{Q}}^* = \Pi_1 \times \Pi_6 = \dot{\mathcal{Q}}/(\rho C_p \Delta T\sqrt{gL_h^5})$ which is the ratio of fire power to the enthalpy rate, and second, Π_4 represents the ratio of the fuel flow rate to the advection rate (Quintiere 2006). Π_{13}^{-1} denotes the Peclet number (Pe) based on the average velocity of the fuel vapor that leaves its surface (Chuah et al. 2011). This definition of Pe represents the burning rate and has been commonly used in flame height discussions (Chuah et al. 2011; Kuwana et al. 2011; Klimenko and Williams 2013).

3. FORMATION OF FIRE WHIRLS

Fire whirls emerge when terrain/domain features (obstructions), and wind coalesce over a strong self-sustaining source of buoyancy (fire plume) and form a concentrated flaming vortex column. A fire whirl is not necessarily comprised of swirling flames within the vortex

column (Countryman 1971), as many cases have been reported to form from hot gases at downwind of large fires (Zhou and Wu 2007; McRae et al. 2013); see figure 1-(b). Hence, given the collective body of evidence on fire whirls, they can be classified in two main types: on-source and off-source. When the whirling flame (vortex column) forms directly over the fuel source, the fire whirl is defined as on-source, and when it forms with an offset from the fuel surface, it is considered off-source (Hartl 2016). Both on-source and off-source types can be found in a quasi-steady or unsteady state. We shall use this classification to describe documented instances of fire whirls in the remaining sections.

Regardless of this classification, fire whirls can also be categorized based on their characteristic length scale, which is most often chosen to be height of the vortex column. Fire whirls with flame heights between $0.1 - 1$ m are defined as small scale (Snegirev et al. 2004), which have been abundantly studied both experimentally and numerically (Emori and Saito 1982; Battaglia et al. 2000b,a; Hassan et al. 2005; Snegirev et al. 2004; Zhou and Wu 2007; Chuah et al. 2009; Lei et al. 2015a; Lei and Liu 2016; Hartl and Smits 2016). Whirls with flame heights between $1 - 10$ m and $10 - \mathcal{O}(100)$ m are categorized as medium and large-scale cases, respectively (Snegirev et al. 2004; Hartl 2016). Even larger events, of the order of kilometers, are documented in the literature that have occurred during large urban conflagrations (Soma and Saito 1991) or bushfires. For instance, a fire-atmospheric event termed pyro-tornadogenesis has been described by McRae et al. (2013).

3.1. Essential conditions for fire whirl formation

For all different types and scales of fire whirls, three crucial factors are essential in their formation, namely a thermally-driven fluid sink, an eddy (vorticity) generation mechanism, and a surface drag force to create a radial boundary layer, such that it facilitates air entrainment to the generated vortex column (Byram and Martin 1962, 1970). The fire acts as a fluid sink, where the generated plume naturally drives horizontal flows radially towards the vortex column. Therefore, the most substantial element in fire whirl formation is the presence of an eddy-generating mechanism.

During mass fires, the possibility of having strong eddies coalescing with fluid sinks and shear forces at the base is high. In these extreme events a variety of natural means exist that can generate the required eddy, such as flow channeled by topological features (Countryman 1971), the interaction of multiple fires or plumes (Liu et al. 2007), the wake of a hill, ridge or large fire plume (Emori and Saito 1982), and generally the transformation of horizontal vorticity into the vertical direction (Church et al. 1980; Forthofer and Goodrick 2011). Examining the definition of vorticity using the Navier-Stokes equations, i.e. $\omega = \nabla \times \mathbf{U}$, may provide better insights on the vorticity generation and cascade through the fire whirl domain. Following Forthofer and Goodrick (2011)'s notation, the vorticity equation reads as

$$\frac{\mathcal{D}\omega}{\mathcal{D}t} = \underbrace{(\omega \cdot \nabla)\,\mathbf{U} - \omega\,(\nabla \cdot \mathbf{U})}_{\text{Tilting \& Stretching}} + \underbrace{\frac{1}{\rho^2}\nabla\rho \times \nabla p}_{\text{Baroclinic}} + \underbrace{\nabla \times \left(\frac{\nabla \cdot \hat{\sigma}}{\rho}\right)}_{\text{Traction forces}} + \underbrace{\nabla \times \mathcal{F}_B}_{\text{Body forces}}, \tag{3.1}$$

where ω denotes the vorticity vector, $\mathcal{D}$ is the material derivative, t is time, p is pressure, $\hat{\sigma}$ is the stress tensor due to viscous effects, and $\mathcal{F}_B$ denotes the body forces. The left-hand side of equation 3.1 represents the temporal and spatial transport of vorticity throughout the domain. In a fire scenario, the generated vorticity is often transported by the ambient flow. On this note, $(\omega \cdot \nabla)\,\mathbf{U}$ describes the tilting of vorticity due to velocity gradients.

This can be directly observed through transitions between horizontal and vertical vortices leading to fire whirl formation (Church et al. 1980; Satoh and Yang 2000). The term $\omega\,(\nabla \cdot \mathbf{U})$ represents the straining effect on the fluid elements due to stretching and/or compressing motions which cause production or dissipation of vorticity. Figure 2-(top) illustrates a schematic of this tilting and stretching process in a nonuniform buoyant velocity field where an eddy-generating mechanism exists. For more theoretical details on the tilting and stretching of vortices during wildland fire scenarios, refer to Sharples et al. (2015) and Simpson et al. (2016). The converging flow in the vortex column of a fire whirl also

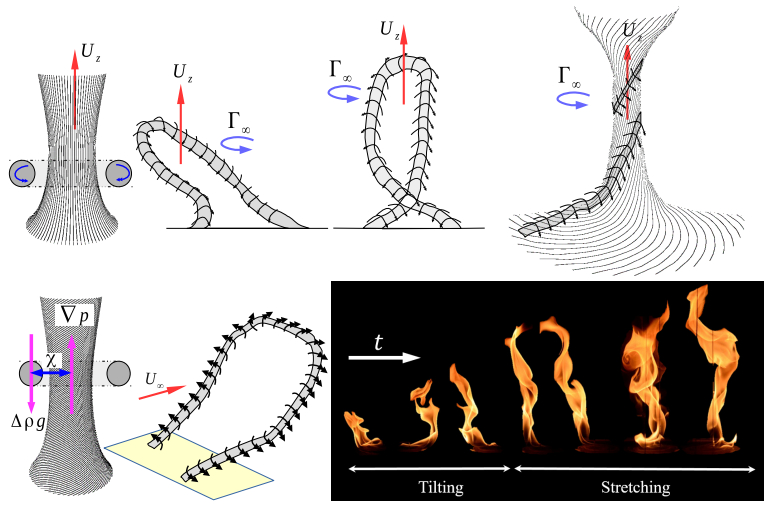

Figure 2

Schematic diagrams of vorticity generation processes, namely tilting and stretching (top), the baroclinic term (bottom-left), and traction forces (bottom-middle), evolving the vorticity field. Also shown is the evolution of the flame sheet through time as a pool fire transitions into a fire whirl which demonstrates the presence of tilting and stretching under controlled laboratory conditions.

concentrates existing vorticity, as shown in figure 2. The Baroclinic term represents the generated vorticity due to misalignment between pressure and density gradients (figure 2-(bottom-left)). In fire whirls, a natural misalignment between pressure and density gradients exists, particularly in the horizontal direction (refer to the later discussion on equation 4.6). In addition, depending on the flow boundary conditions and configurations, the term $\nabla \times (\nabla \cdot \hat{\sigma}/\rho)$ accounts for the production or dissipation of vorticity due to imposed traction forces on a fluid's elements. A typical vortex tube generated due to traction forces is shown in figure 2-(bottom-center). Finally, the body forces term in equation 3.1 takes into account variations of the vorticity field due to external body forces such as gravity or magnetic fields. A schematic of fire whirl development through time is demonstrated in figure 2-(bottom-left) where all these effects act together in a complex manner.

The aforementioned conditions are observed in nature or replicated in laboratory experiments under different configurations. A brief summary of documented cases are given below.

3.2. Open Configurations

Most known open fire whirl configurations, including on and off-source, quasi-steady and unsteady, can all be observed over an L-shaped fire in cross-flow as shown in figure 3-(a). This configuration is similar to the Hifukusho-ato fire whirl (HAFW), which occurred

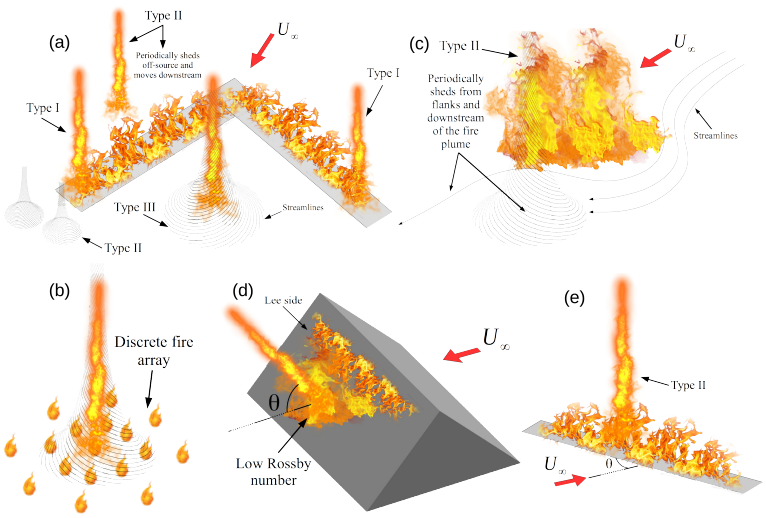

Figure 3

Shown are various open configurations which can generate fire whirls. (a) An L-shaped configuration under cross-flow, (b) a discrete fire array, (c) a large fire in cross-flow which can shed fire whirls on its flanks or in its wake, (d) the lee side of a slope over which an inclined fire whirl can form, and (e) a line fire in cross-flow.

following a devastating earthquake in Tokyo in 1923, killing almost 38,000 people (Soma and Saito 1988, 1991; Kuwana et al. 2007). Three types of whirls are found in this configuration; a stable on-source fire whirl on both ends of the 'L', unsteady fire whirls which travel along the edge or flanks of the fire and shed periodically in its wake, and a stable off-source whirl which forms within the unburnt region between the 'L'. The first type, Type I, is most like enclosed fire whirls discussed in the following section, being both on-source and quasi-steady. These types could also be formed by array of multiple fires, with or without cross-flow, where any asymmetry in the flow or geometry may casue/amplify the swirl which generates a whirl (Zhou and Wu 2007); see figure 3-(b). This behavior is thought to have been observed following the deliberate fire-bombing of Dresden and Hamburg during World War II (Soma and Saito 1991). The second type, which is off-source and periodic in nature, is also seen on the flanks of large wildfires as well as in the wake following large bent-over plumes. These have been called "Dessens" fire whirls (DFW) in the past due to their similarity to whirls observed downstream of a large-scale experiment by Dessens (1962); a schematic of such cases is shown in figure 3-(c). Finally, fire whirls known as Type III are formed in off-source regions with either flames or merely hot cases under cross-flow, similar to the HAFW whirl described above.

Other fire whirls include those seen to form on the lee side of a hill following a wildfire. These whirls are similar to Type II or III whirls, depending on whether they are quasi-steady, the location of the fuel and obstruction, and the orientation of ambient flow. In general, strong vorticity is generated behind an obstruction in cross-flow, such as a hill, which has been known to create re-circulation regions that can drastically modify fire spread at the top of hills (Sharples et al. 2015); however, when vorticity becomes tilted upward, one or more fire whirls may form. Fire whirls have also been seen to arise from interactions between a line fire and cross-flow, where an unsteady, on-source whirl can form under specific velocity, orientation and fire sizes. These fire whirls may travel along a line fire similar to Type II fire whirls which form on the flanks of larger fires (Kuwana et al. 2013; Zhou et al. 2016).

Scale-modeling experiments have revealed, for a variety of configurations, a strong dependence of the formation of fire whirls on the ambient cross-flow velocity. For instance, formation of a Type-III fire whirl formed in a L-shaped configuration has been found to depend on a critical cross-flow velocity (Soma and Saito 1991),

$$U_{cr} = L_h^{3/8} \dot{m}^{1/4}. \tag{3.2}$$

An equivalent non-dimensional relationship was later proposed by Kuwana et al. (2008) as

$$\frac{U_{cr}}{\sqrt{gL_h}} \sim Fr_f^{\eta/2}, \quad \eta = 0.3, \tag{3.3}$$

where $Fr_f = \dot{m}^2/(\rho_\infty^2 g L_h)$ is the fuel's Froude number, and ρ_∞ is the air density at ambient temperature. In addition, other correlations between $U_z/\sqrt{gL_h}$ and Fr^η are reported for fire whirls over line fires and type III cases, in which the values of η vary (Kuwana et al. 2013).

3.3. Enclosed Configurations

Since fire whirls in nature are mostly violent and erratic, there is, as of yet, no unique parameters that can quantify and describe the necessary formation conditions in the open, although some empirical correlations based on dimensional analysis are presented (e.g. equations 3.2 and 3.3). Systematic studies of this nature are carried out in enclosed configurations where either horizontal barriers or mechanical means have been used to induce the required circulation for fire whirl formation. Schematics of several common enclosed configurations are illustrated in figure 4.

Most reported laboratory studies have utilized walls to constrict airflow so that it enters into the test region tangentially. In these configurations, the fuel source is often located at the bottom center of two halves of an offset hollow cylinder, illustrated in figure 4-(a). Hot gasses exit the top opening and ambient air is entrained tangentially into the chamber through the intake(s). As the circulation strength increases, the spiraling flame tilts and eventually elongates such that its axis coincides with the central axis as a sustainable vertical column of whirling flame (Byram and Martin 1962, 1970). This delivers a quasi-steady on-source fire whirl which has been studied extensively (Hassan et al. 2005; Chuah et al. 2011; Kuwana et al. 2011; Hayashi et al. 2011; Hartl and Smits 2016; Xiao et al. 2016; Wang et al. 2016; Satoh and Yang 1996; Satoh et al. 1997; Lei et al. 2011; Zhou et al. 2013; Dobashi et al. 2015). Square enclosures with tangential slits have also been used (figure 4-(b)), however they may introduce redundant eddies into the system, due to the recirculation zones at the corners (Hartl and Smits 2016). Others have modified the setup by installing blowers or air intake at the base in order to provide sufficient air into the chamber (Byram and Martin

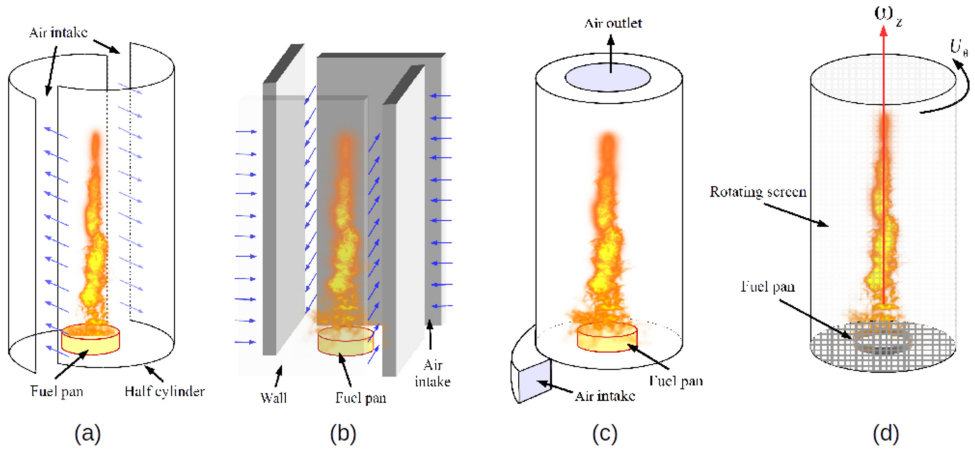

Figure 4

Four types of enclosed configurations for generating fire whirls in the laboratory including two half-cylinders offset with slits (a), four walls with slits (b), circular intake (c), and a rotating mesh setup (d).

1962, 1970; Muraszew et al. 1979) or using variations with six or more walls (Chuah et al. 2011; Dobashi et al. 2015). Figure 4-(c) shows a schematic of the setup with an air intake at the base. Using these configurations, the circulation strength and the entrainment can be varied by changing the diameter of the chamber or adjusting the slit spacing.

Rather than using slits in a solid enclosure, vorticity can also be added to the system via a rotating screen. This setup has been advantageous in that the circulation strength within the domain can be varied through adjustment of the angular velocity of the screen as shown in figure 4-(d). This approach was first adopted by Emmons and Ying (1967) and as a result is often called an Emmons-type fire whirl generator. Since the strength of eddies can be controlled, this approach is favorable for theoretical analysis of the fire whirl structure (Chuah and Kushida 2007), although the domain instrumentation and measurement are more difficult than in fixed-frame setups. This method has also been employed in a series of experiments where multiple equidistant fire whirls were generated between two vertical screens that were both parallel to a propane line fire and moving in opposite directions (Lee and Garris 1969). There are also other mechanical methods that can lead to the generation of whirling flames including the use of air curtains and tangentially-oriented blowers at the fuel surface (Byram and Martin 1970; Mullen and Maxworthy 1977; Wang et al. 2015). One advantage of these techniques is that restrictive walls are not necessarily needed which enables easier experimental probing. However, maintaining the flow symmetry inside the domain is more challenging than other methods.

4. INNER STRUCTURE OF THE FIRE WHIRL

To date, most of what is known about the inner structure of fire whirls comes from the mathematical and experimental characterization of quasi-steady on-source cases at laboratory scales. The inner structure of such fire whirls can be approximated as a three dimensional axisymmetric flow as shown in a schematic of the velocity field on figure 5.

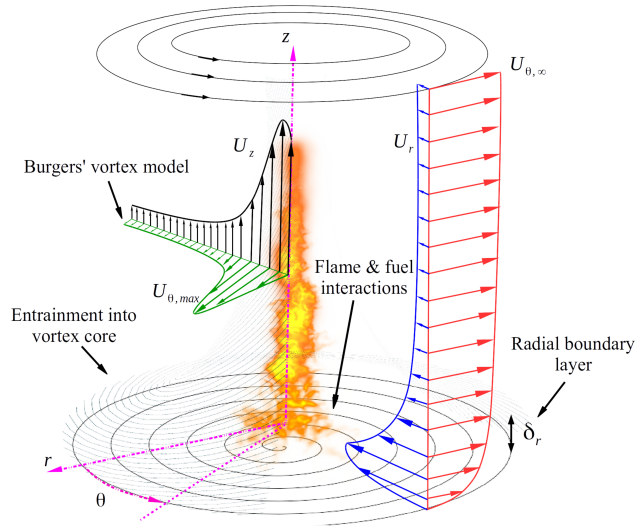

Figure 5

A schematic of the typical velocity field of a quasi-steady on-source fire whirl.

In order to answer fundamental questions about fire whirls and examine their inner structure, it is necessary to have a thorough theoretical model that describes the generated vorticity, velocity, and temperatures fields. While this does not yet exist, theory of the secondary flow arising from a fluid's rotation over heated solid boundaries does and is called the Bödewadt (1940) problem, previously treated by Stewartson (1953) and Nydahl (1971). However fire, which continuously modifies the swirling flow, has not been included in the problem and there are also issues with the stability of the proposed solutions. As for fire whirls, turbulent plume theory was applied by Emmons and Ying (1967) to a modified model of a free vortex over a ground plane, i.e. 3D axisymmetric flow. In this section, the vorticity field will be described first, followed by geometric characterization of the structure. Then, the velocity field of fire whirls can be explained along with their thermal composition.

4.1. Vorticity Field

Experimental measurements for both small (Emmons and Ying 1967; Soma and Saito 1991) and medium scale (Muraszew et al. 1979; Lei et al. 2011) enclosed fire whirls reveal that the azimuthal velocity U_θ increases linearly with radius inside the whirl column (vortex core), and decreases proportional to $1/r$ outside of it. This indicates that the fire whirl core can be approximated as a rotating solid body and outside of the core the flow field is approximately a free vortex. This is further confirmed by PIV (Hassan et al. 2005; Matsuyama et al. 2004; Akhmetov et al. 2007) and stereo-PIV measurements (Smits et al. 2012; Wang et al. 2016; Hartl and Smits 2016). With respect to the vorticity field, other experimental results by Lei et al. (2015b), conducted in a fixed-frame four-walled enclosure, suggest that the fire whirl domain can be divided into three distinct regions in the radial direction. Respectively, from the center of the whirl, these include the vortex core, the quasi-free vortex, and the near-wall regions. The first two vorticity zones were previously identified, while the near-

wall zone forms due to the experimental configuration, according to Lei et al. (2015b). The near-wall zone is rich in vorticity which conserves the vorticity content of the whirl column by imparting eddies of different scales into the whirl, primarily through the radial inflow boundary layer at the base.

Prior knowledge of the vorticity field delivers a better understanding of the velocity distribution in the domain. Hence, some studies (Byram and Martin 1962; Hassan et al. 2005) adopt the Rankine vortex model (Batchelor 1953, 2000; Kundu et al. 2008) to describe the velocity field of the fire whirl while others (Chuah et al. 2009; Lei et al. 2011; Kuwana et al. 2011; Lei et al. 2015b) report that the Burgers vortex model (Burgers 1948) fits best with their observations. Also, the Sullivan vortex model (Donaltson et al. 1960) is utilized by Chuah and Kushida (2007) to describe the velocity components of the fire whirl. Assuming that Γ_∞ is the ambient circulation and b_w is radius of the vortex (whirl) core, equations 4.1 and 4.2 show the radial profile of the azimuthal velocity along with the associated circulation for the Rankine (Kundu et al. 2008) and Burgers (Burgers 1948) vortex models, respectively.

$$U_\theta(r) = \begin{cases} \left(\dfrac{\Gamma_\infty}{2\pi b_w^2}\right) r, & r \leq b_w \\ \left(\dfrac{\Gamma_\infty}{2\pi}\right) \dfrac{1}{r}, & r > b_w \end{cases} \qquad \Gamma(r) = \begin{cases} \left(\dfrac{\Gamma_\infty}{b_w^2}\right) r^2, & r \leq b_w \\ \Gamma_\infty, & r > b_w \end{cases} \tag{4.1}$$

$$U_\theta(r) = \frac{\Gamma_\infty}{2\pi r}(1 - e^{-r^2/b_w^2}), \qquad \Gamma(r) = \Gamma_\infty(1 - e^{-r^2/b_w^2}) \tag{4.2}$$

In Burgers representation, equation 4.2, the maximum value of azimuthal velocity occurs at $r \approx 1.12091 b_w$ (Kundu et al. 2008; Hartl 2016). Figure 6-(a), compares the distribution of azimuthal (tangential) velocity with respect to distance from the vortex column's centerline axis for different vortex models against stereo-PIV measurements of Hartl and Smits (2016) and Hartl (2016). Even though some studies (Hayashi et al. 2011; Klimenko and Williams 2013) reported that the Burgers vortex model does not provide an adequate description for the radial distribution of azimuthal velocity, the available evidence, collectively, suggests that it is the best fit for a quasi-steady on-source fire whirl (Smits et al. 2012; Lei et al. 2015b; Wang et al. 2016; Hartl and Smits 2016; Hartl 2016).

4.2. Geometric Characteristics

Before further discussion on the velocity field and variation of other parameters, it is important to define the geometric characteristics of the fire whirl in the vertical (z) and radial (r) directions.

4.2.1. Along the z-direction. Three distinct regions have been defined along the z-direction including the continuous flame, intermittent flame, and plume regions (Lei et al. 2013, 2015b). A schematic of these regions is shown in figure 7. The continuous region represents the fire whirl's core height where the axial flow accelerates upward to the maximum axial centerline velocity. This is observed to occur at $z/H = 0.7$ where H is the observed flame height of the fire whirl (Lei et al. 2013, 2015b). Relative to pool fires in a quiescent environment, the height of the continuous flame region in fire whirls is by far greater (Lei et al. 2011). The intermittent region usually occurs at $0.7 \leq z/H < 1.22$, where $z/H = 1.22$ corresponds to the luminous tip of the fire whirl. Velocity fluctuations are significant within this region and the centerline axial velocity decreases rapidly. Next, the plume region

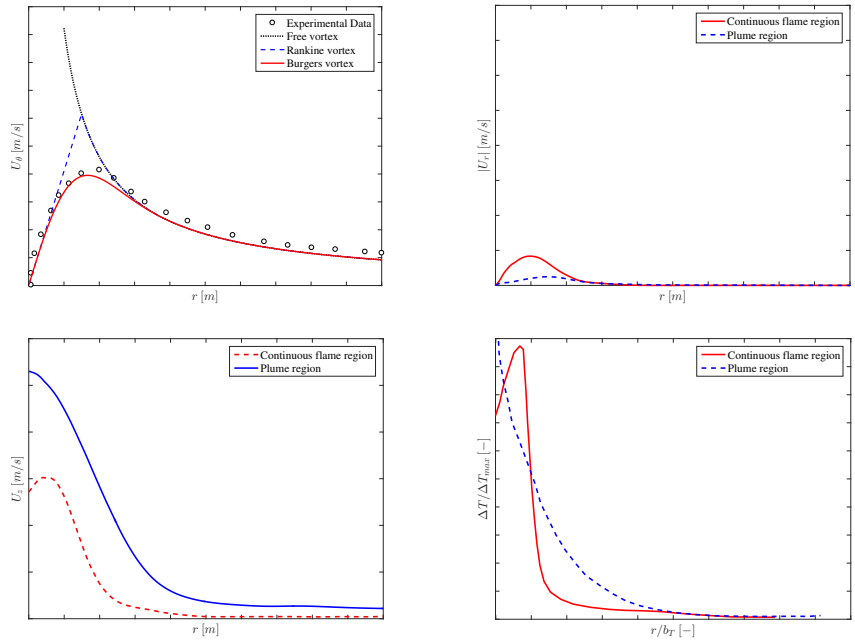

Figure 6

Velocity profiles predicted and measured for the inner and outer structure of an on-source, stationary fire whirl. (top-left) Azimuthal velocity as a function of radius including theoretical predictions and experimental data from Hartl (2016); Hartl and Smits (2016), and (top-right) radial velocities within the continuous flame and plume regions. Also, (bottom-left) axial velocities measured within the continuous flame and plume regions from Hartl (2016), and (bottom-right) normalized excess temperature againts normalized radial distance with b_T measured within the continuous flame and plume regions by Lei et al. (2015b).

extends beyond the visible tip of the whirl core, where the axial velocity decelerates to the ambient flow. Customarily, the plume behavior is characterized based on flow conditions at its virtual origin (Morton et al. 1956; Turner 1979; Hunt and Kaye 2001). So far, location of the virtual origin within the whirling column of a fire whirl has not been measured or discussed. Instead, a vertical distance that is adjusted by the maximum flame height at the intermittent region (H_{if}) has been used for characterizing the flow attributes. Lei et al. (2015b) formulated this length scale as $L_v = (z - H_{if})/H$.

4.2.2. Along the r-direction. An accurate description of the fire whirls' inner structure is intimately tied to proper description of the whirl core and plume radius. To this end, the mean plume buoyancy and width are obtained by extending classic plume theory (Morton et al. 1956; Turner 1979) on experimental measurements of fire whirls (Emmons and Ying 1967). Adopting the standard entrainment assumption for flow in an unstratified environment where the Boussinesq approximation is applicable, and following the notation of Hunt and Kaye (2001), the fluxes for a quasi-steady 3D axisymmetric fire whirl can be written as

$$Q = 2\pi \int_0^\infty \rho U_z r dr, \qquad M = 2\pi \int_0^\infty \rho U_z^2 r dr, \qquad F = 2\pi \int_0^\infty (\rho_0 - \rho) U_z r dr, \quad (4.3)$$

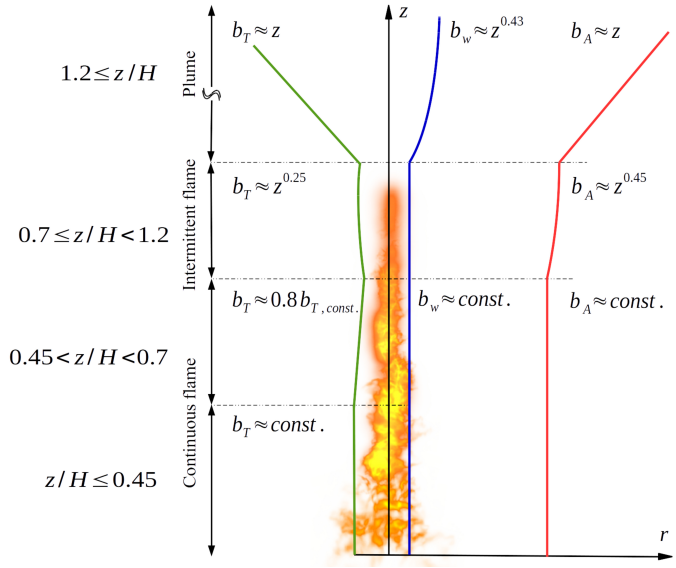

Figure 7

Schematic of different regions identified along the axial and radial diractions. According to Lei et al. (2015b), for all fire sizes, on average, the radius based on axial velocity (b_A) is greater than the radius based on the excess temperature (b_T) and this itself is greater than the radius based on the azimuthal velocity (b_W), that is throughout the height of a fire whirl $b_A > b_T > b_W$.

where Q, M, and F are the volume, axial momentum, and buoyancy fluxes along the z direction, respectively, and ρ_0 is the reference density. Similar to Tohidi and Kaye (2016), Q, M, and F can be written in the form of specific fluxes as $\hat{Q} = Q/(2\pi\rho_0)$, $\hat{M} = M/(2\pi\rho_0)$, and $\hat{F} = F/(2\pi\rho_0)$ (Lee and Chu 2012). One can map the conservation equations with these specific fluxes and integrate them using the standard entrainment model that is incorporated with the fire whirl radius (b_A) and the mean plume buoyancy $\Delta\gamma$, which can be shown as

$$b_A = \hat{Q}/\sqrt{\hat{M}} \tag{4.4}$$

and

$$\Delta\gamma = \frac{\rho_0 \hat{F}\hat{Q}}{\hat{M}}\chi. \tag{4.5}$$

It should be noted that the standard entrainment model only couples the radial variations of the inflow with shearing effects due to the axial velocity. Thus, more sophisticated entrainment models are needed. Also, unlike other studies (Emmons and Ying 1967; Lei et al. 2015b), using equation 4.4 does not require the top-hat assumption for the axial velocity profile, which effectively decouples the flame length from the flow structure (Kuwana et al. 2011). In equation 4.5, χ can be interpreted as the density deficit length scale within or beyond the fire whirl core,

$$\chi = \frac{1}{\rho_0}\int_0^\infty \rho r dr. \tag{4.6}$$

This parameter (χ) may represent a length scale in the radial direction within which the total density deficit is accumulated, although, to the authors' best knowledge, it is not yet

discussed in the fire whirl literature.

Neglecting small viscous forces, i.e. $\mathcal{O}(\mu) \approx 0$, within the rigid-body rotating core of the fire whirl and considering negligible vertical diffusion for heat and species, Emmons and Ying (1967) decoupled the azimuthal velocity from buoyancy and axial velocity leading to a set of ordinary differential equations in terms of U_z, U_r, b_A, and $\Delta\gamma$. With a constant entrainment coefficient the proposed model fails to predict the growth width with height, therefore a variable entrainment coefficient was used. In a different approach, others define b_A as the radial distance from the whirl's vertical axis at which the local axial velocity, U_z has declined to a fraction of the maximum recorded value at the same height. For the continuous flame region, this is equal to 0.5 and 0.3 in Lei et al. (2015b) and Wang et al. (2016), respectively. As equation 4.4 suggests, b_A varies with height. Lei et al. (2015b)'s measurements show that, when $\dot{\mathcal{Q}} \geq 200\,kW$, the whirl's upward flow is constrained by an external downward flow which makes b_A relatively constant for the first half of the continuous flame region, i.e. $z/H \leq 0.45$. Then, b_A increases in the upper half of the continuous region and even decreases with higher rates in the intermittent and plume regions. A power-law correlation of the form $b_A = 3.08\dot{\mathcal{Q}}^{0.26}$ has been observed by Lei et al. (2015b), where b_A is in cm and the heat-release rate is in kW. Figure 7 shows spatial variations of b_A for a typical quasi-steady on-source fire whirl.

Similarly, the temperature core radius, b_T, is defined as the radial location where excess temperature declines to half of the maximum recorded value at that height (Lei et al. 2015b). Due to cyclostrophic balance, flame pulsations are suppressed in the radial direction causing the flame radius to be relatively constant through the first half of the continuous flame region, provided that $\dot{\mathcal{Q}} > 150\,kW$. Therefore, b_T is a reasonable candidate to describe the flame shape in the axial direction (Lei et al. 2015b). Beyond the first half of the continuous flame region, up to the end of the intermittent flame zone, b_T declines to a minimum which is approximately 80% of the average recorded value. This implies that a considerable fraction of convective heat is constrained and transported upward in the vortex core. After the intermittent region, b_T grows with height (L_v). Lei et al. (2015b) also found an empirical correlation, $b_T = 2.19\dot{\mathcal{Q}}^{0.31}$, where b_T is in cm and the heat-release rate ($\dot{\mathcal{Q}}$) is in kW. Variations of b_T with respect to height are shown in figure 7.

A qualitative comparison of b_A with b_T shows that, for the lower half of the continuous flame region, b_A is slightly smaller than b_T. This illustrates the constraining effects of the downdraft flow within the domain (Lei et al. 2015b). However, for a wide range of heat-release rates, b_A is always larger than the measured b_T at the same height. This holds true along the three regions of whirl core and implies that the axial velocity core expands faster than the temperature core.

Also, the mean whirl (vortex) core radius (b_w) is characterized such that, beyond it, the circulation is nearly constant, i.e. the tangential velocity is maximum (Lei et al. 2015b; Hartl and Smits 2016). The mean vortex core radius is correlated with the heat-release rate as $b_w = 2.36\dot{\mathcal{Q}}^{0.28}$, where b_w is in cm and $\dot{\mathcal{Q}}$ is in kW. Also, b_w is found to be always less than b_T and b_A. With respect to variations in height, Lei et al. (2015b) observed that b_w is relatively constant for $z/L_h \leq 1.0$. From the experimental findings of Lei et al. (2015b), one can infer that, on average, $b_A > b_T > b_w$ throughout the height of the fire whirl. In addition, b_w increases with height in the intermittent and plume regions as shown in figure 7-(b).

4.3. Velocity Field

Knowing the geometric characteristics of fire whirls, their velocity field, which is closely related to the radial inflow boundary layer at base, entrainment, and turbulence suppression mechanisms can be described.

4.3.1. Radial Velocity Component, U_r. As the fluid particles adjacent to the solid boundary decelerate, the cyclostrophic balance between the centrifugal force and the pressure gradient generated by buoyancy and circulation is disturbed. This leads to formation of the radial boundary layer towards the center of the whirl column (Byram and Martin 1962, 1970; Ying and Chang 1970; Lei et al. 2015b; Muraszew et al. 1979; Hayashi et al. 2011; Hassan et al. 2005). The isothermal model of Ying and Chang (1970) also shows that the maximum radial velocity occurs adjacent to the surface and reverses direction close to the upper parts of the boundary layer, indicating presence of a circulation zone (Hartl and Smits 2016). Also, other PIV measurements (Hassan et al. 2005) show that outside of the whirl core the radial velocity rises to a maximum value which is smaller than the tangential and axial velocity at the same heights. On this note, the maximum radial velocity is linearly correlated with circulation (Ying and Chang 1970; Hartl 2016). The recirculation region thickness near the base is reported to extend up to 15 mm above the fuel (burner) surface for all combinations of the burning rate and ambient circulation in experiments by Hartl and Smits (2016). Within this region, the magnitude of the average radial velocity is considerable, for both pool and burner fire beds, although it drastically reduces to negligible values for $z > 15$ mm. Figure 6-(top-right) shows a typical distribution of the radial velocity in the r direction.

4.3.2. Azimuthal Velocity Component, U_θ. Given the variations of b_w with respect to height and heat-release rate, the maximum azimuthal velocity ($U_{\theta_{max}}$) tends to increase between $0 \leq z/L_h \leq 1.25$ and decrease beyond $z/L_h = 1.25$ (Lei et al. 2015b). After this region, the rate of decline of ($U_{\theta_{max}}$) is reported to be equal for all fire loads. In the continuous flame zone, $U_{\theta_{max}}$ correlates with heat-release rate as $U_{\theta_{max}} = 1.58\dot{\mathcal{Q}}^{0.22}$. Despite these variations, the normalized azimuthal velocity ($U_\theta/U_{\theta_{max}}$) versus the normalized radial distance (r/b_w) is self-similar, with insignificant scatter around the Burgers vortex model; see figure 6-(top-left). This holds true for a wide range of $\dot{\mathcal{Q}}$ and at any arbitrary height (Byram and Martin 1970; Hassan et al. 2005; Akhmetov et al. 2007; Wang et al. 2016; Hartl and Smits 2016).

4.3.3. Axial Velocity Component, U_z. Using specific fluxes, the axial velocity above the boundary layer can be obtained by $U_z = \hat{M}/\hat{Q}$. Alternatively, an analytic expression for the axial velocity is derived (Lei et al. 2015b) by coupling circulation and buoyancy as

$$\frac{\partial U_z^2}{\partial z} = \frac{2(T_{C.L.} - T_\infty)}{T_\infty} g + \frac{\partial}{\partial z}\left[\frac{U_\theta^2}{2}\left(\frac{1}{\eta_1} + \frac{\rho_\infty}{\rho}\frac{1}{\eta_2}\right)\right], \qquad z \geq \delta_r, \tag{4.7}$$

where $T_{C.L.}$ is the centerline temperature, δ_r is the thickness of the radial boundary layer at the base, η_1 and η_2 are exponents of the power-law fits to the azimuthal velocity distribution in the radial direction through the solid-body rotating core and the free-vortex zone, respectively. Note that equation 4.7 is valid for $z > \delta_r$, therefore it can be integrated from δ_r to any arbitrary height in order to give the excess axial velocity, i.e. $(U_z^2 - U_{z|\delta_r}^2)_{|r=0}$. Equation 4.7 indicates that, in fire whirls, the centerline axial velocity not only depends on buoyancy, but also the radial distribution of the azimuthal velocity (circulation). Hence,

within the fire whirl core, vorticity, temperature, and axial velocity are all coupled (Lei et al. 2015b).

It has been shown that the circulation in fire whirls, compared to non-swirling pool fires with the same source characteristics, causes an initial reduction of the centerline axial velocity due to the formation of a viscous region in the boundary layer (Zhou and Wu 2007). This has been confirmed for various levels of circulation in Zhou and Wu (2007)'s experiments. Hence, a fire whirl flame in the continuous region consists of both a viscous and inviscid part which is buoyancy-dominated. This is also observed in Lei et al. (2015b)'s experiments where it is found that the axial centerline velocity varies with height as $U_{z|r=0} \sim z^{1/3}$ within the continuous flame region and $U_{z|r=0} \sim z^{-2/3}$ throughout the intermittent region before the fire whirl decelerates back to the plume zone. Consistent with buoyancy-dominated flows in which inertia is balanced by buoyancy (Thomas 1963), using dimensional analysis, Hartl and Smits (2016) argues that the centerline axial velocity in the continuous flame region of fire whirls scales as $z^{1/2}$ and, as the height increases to the plume region, fire whirls behave more like a buoyant plume with weak swirl rather than a strong swirling jet. On this matter, the expansion rate of the fire whirl plume can be calculated based on the axial velocity, azimuthal velocity, and the excess temperature. The stabilizing effects of circulation, however, deliver smaller expansion rates relative to swirling jets ejected to the quiescent ambient (Beér and Chigier 1972); see section 5.3. As the axial velocity decelerates to the plume region, due to absence of the flame sheet, the radial density stratification and consequently the cyclostrophic balance is disturbed. Thus, the influence of circulation is reduced and, subsequently, the straining effects of the vortex column decreases. This expands the fire whirl plume radius such that the faster increasing rate of b_A leads to a more rapid decay of $U_{z|r=0}$. A better understanding of these processes can be obtained by following vertical variations of the axial velocity profile and b_A shown in figure 6-(bottom-left) and figure 7, respectively.

The radial distribution of axial velocity is believed to follow the temperature distribution along the r-direction (Emmons and Ying 1967). This is confirmed by Lei et al. (2015b)'s measurements, where it is found that, within the continuous flame region, the maximum axial velocity does not occur at the centerline axis. This suggests a hump-like distribution in the r-direction. As the height increases, the hump-like profile becomes a plateau, with no strict self-similarity between the radial profiles (Emmons and Ying 1967; Lei et al. 2015b). Through the intermittent flame zone, the plateau-type velocity profile takes a Gaussian form with its maximum value at the centerline. PIV measurements by (Hassan et al. 2005; Wang et al. 2016) reveal a self-similar Gaussian radial profile for the normalized axial velocity against the normalized radius, regardless of the circulation strength and height. Also, the experimental measurements by Lei et al. (2015b) suggest that the data's scatter around Gaussian fits is less within the plume region compared to the intermittent flame zone; see the vertical variations of the axial velocity profile in the r-direction shown in figure 6-(bottom-left).

4.4. Thermal Composition

4.4.1. Temperature, T. Emmons and Ying (1967) first measured the radial temperature distribution of a liquid (acetone) pool fire whirl at a single height and reported a hump-like profile in the r-direction as shown on figure 6-(d). This has also been seen in measurements by Lei et al. (2011, 2015b) and Wang et al. (2015). The maximum recorded temperatures

occurred near/within the flame sheet, where this value was 1.6 times the centerline temperature, i.e. $T_{max} - T_\infty \approx 1.6T_{r=0}$. This implies that the fire whirl has a fuel-rich core with no active combustion reaction (Wang et al. 2015) which significantly influences the radial temperature distribution throughout the continuous flame region (Zhou et al. 2013). The radius of this core is defined as the location where $T = T_{max}$ (Emmons and Ying 1967). Outside this core, the temperature sharply decreases (Muraszew et al. 1979). In addition, the radial gradient of temperature decreases with increasing height due to continuous heat transfer from the reactive flame sheet to the thermal core (increase in b_T) (Lei et al. 2015b). Increasing in height to the intermittent flame region and beyond, shifts the maximum temperature towards the whirl's centerline, and forms a Gaussian profile regardless of the heat-release rate. These Gaussian profiles within each flame region are self-similar. This suggests that the fire source dimension (D_0) and heat-release rate ($\dot{Q}$) do not, considerably, affect the radial distribution of temperature at high elevations (Lei et al. 2011, 2015b; Wang et al. 2015). Moreover, the flame temperature in whirling flames compared to their non-whirling counterparts has been measured to be 1.2 times higher (Grishin et al. 2005). This behavior is attributed to higher diffusion rates, due to a better oxygen supply in the elongated combustion region in fire whirls.

On the same note, since turbulence is suppressed in fire whirls, which subsequently reduces mixing with cold ambient air throughout the free-vortex column, temperature decreases slowly with height in the continuous flame region. Throughout this region, there is a correlation between excess temperature and the normalized height as $\Delta T \sim (z/H)^{-0.06}$ (Lei et al. 2015b). The exponent of temperature decay later decreases to -1.79 for the intermittent flame region. In the plume, the variation of excess temperature along the z axis (increase in L_v) scales with $z^{-5/3}$ (Mullen and Maxworthy 1977; Lei et al. 2011), which is consistent with classic observations for non-rotating turbulent plumes. Also, Lei et al. (2015b) shows that there is a power-law correlation between the excess temperature decay and L_v, where the fitted exponent varies between -1.51 to -0.09 for different heat-release rates at the source. This scatter can be attributed to different turbulent dissipation rates within the plume region. These trends are also reported by Wang et al. (2015), yet with slightly different exponent values.

4.4.2. Radiation. In order to evaluate the radiative heat flux from fire whirls to external surroundings, the whirl has often been assumed to be a homogeneous black-body emitter (Zhou et al. 2011), similar to studies from pool fires (Hamins et al. 1996). Two models have been proposed by Zhou et al. (2011, 2014) which show that there is a considerable variation in the radiant heat flux profile as height increases. In fire whirls with various pool sizes, the radiative heat flux increases throughout the continuous flame zone up to $z/H = 0.4$ and then decreases rapidly beyond it (Zhou et al. 2011; Wang et al. 2015). The decline of radiative heat flux in the plume region is faster than in the intermittent zone, similar to non-swirling pool fires, where the corresponding height through which the radiative heat flux increases is $z/H = 0.5$ (Hamins et al. 1996). As expected, it is reported that the radiative heat flux decreases monotonically in the radial direction.

5. GOVERNING PROCESSES

Scaling laws, based on the influential parameters described in Section 2, have been established to describe some of the underlying processes that govern the structure of quasi-steady

on-source fire whirls, which will be reviewed here.

5.1. Circulation

Circulation is, indeed, the major factor that distinguishes fire whirls from non-swirling fires. Variations in temperature, height, and the velocity field (in particular the axial velocity), are directly interrelated with circulation. In this regard, utilizing dimensional analysis, it is found that the axial velocity and temperature scale with the fire power (P). This is analogous to the (virtual) point source in turbulent plumes, and implies that $U_z \sim P^{1/3}$ and $\Delta T \sim P^{2/3}$ (Mullen and Maxworthy 1977). Note that the imparted power into the system has a direct relationship with buoyancy as $\hat{F} = (Pg)/(\rho_0 C_p T_\infty)$, given that temperature localization is allowed (Lee and Chu 2012). Resulting from the same analysis, Mullen and Maxworthy (1977) found that the vortex core diameter (D_w) varies linearly with the core Reynolds number (Γ/ν) and the boundary-layer thickness (δ_r). It is also shown that the circulation is independent of height (Mullen and Maxworthy 1977; Hartl and Smits 2016). The fire whirl core structure varies sporadically, but due to constant circulation strength the outer flow apparently adjusts and sustains itself in the vertical direction relative to the core behavior (Mullen and Maxworthy 1977) .

Considering circulation effects on the axial velocity, in a general non-swirling pool fire, the Froude number based on the axial velocity is constant (McCaffrey 1979). However, this is not the case for fire whirls as Zhou et al. (2011) argues that both buoyant plume theory and the circulation-induced vortex should be included in the dimensional analysis. This leads to $Fr \sim (\Gamma/\sqrt{gz^3})^\eta$, where η is found to be 0.22 and 0.77 through the continuous flame region and plume, respectively. However, this scaling seems to be inappropriate since the circulation in the free vortex region is typically constant along the vertical direction (Lei et al. 2011; Hartl and Smits 2016). Hartl and Smits (2016) defined the Froude number based on the centerline axial velocity as $U_{z|r=0}/\sqrt{gz}$ and assumed that Fr and circulation are independent of height. Dimensional analysis of their PIV results led to $Fr = 1.65(\dot{\mathcal{Q}}^* L_h^*)^{-0.18}$ where $L_h^* = L_s/D_c$ is the normalized horizontal length scale, L_s is the gap size in their half cylinder setup, and D_c is diameter of the cylinders. It is shown that this Froude number becomes invariant to large values of $(\dot{\mathcal{Q}}^* L_h^*)$. Therefore, the centerline axial velocity is independent of $(\dot{\mathcal{Q}}^* L_h^*)$, i.e. $U_{z|r=0} \sim z^{1/2}$ as mentioned in section 4.3.3.

The influence of circulation strength on the fire whirl's burning rate and flame height are examined through Kuwana et al. (2011)'s experiments where weak and strong circulations were applied to both burner and pool-source fire whirls. Given that the diameter of the burner and pool source were the same (0.3 cm), it is found that strong circulation increases the burning rate and flame height in both pool and burner fire whirls. However, weak circulation only increased the burning rate of the pool source, up to three times the original value, and did not significantly change its flame height. This is due to the fact that the burning rate in the burner fire whirl is constant, whereas, in the pool fire whirl, even a slight circulation increases the heat feedback form the flame sheet to the fuel surface at the base and subsequently increases the burning rate.

Low Rossby number fire whirls, namely those with high circulation, are believed to be rotation-controlled. This is examined on inclined fire whirls on a slope under strong circulation by Chuah et al. (2011). The experimental evidence suggests that low Rossby number fire whirls are dominated by rotation ($Ro \ll Fr$), in that buoyancy has less contribution to the flow structure. Also, a linear correlation is found between H/D_0 and $Pe/(16f)$, where

f is the stoichiometric mass ratio. This implies that the flame height (H) is independent of the inclination angel and buoyancy. In addition, viscous core effects on the outer regions are incorporated in an analytic model developed by Chuah et al. (2011), which was later expanded upon by Klimenko and Williams (2013) employing the strong-vortex approximation and its compensating regime. Although the analytical model is decoupled from density stratification throughout the domain, it shows that the entrainment flow in low Rossby number fire whirls approaches the compensating regime, which is not best described by the Burgers vortex model (Klimenko 2014). As a result, any change in U_z and U_r (the flow structure) triggers changes in the mixture fraction leading to variations in the flame height. Far-field asymptotic solutions of Klimenko and Williams (2013)'s model are in good agreement with experimental data. Further, Zhou et al. (2016) documented nine flame patterns which resulted from the change in external circulation strength and heat-release rate of buoyant diffusion flames in a rotating screen setup. As circulation increased (angular velocty of the screen increased), flames transitioned from a free buoyant flame to one that was inclined and, finally a fire whirl, however even after this transition, the whirl continued to transition to different shapes until it finally became irregular and extinguished. Using a two half-cylinder experimental setup where circulation is not mechanically generated, Hartl and Smits (2016) found that beyond the entrainment zone at the base, circulation may be dependent on mass entrainment for stoichiometric combustion.

5.1.1. Height. Relative to non-swirling fires, the most conspicuous feature of fire whirls is the increase in flame height, where a 10- (Emmons and Ying 1967) to 30- (Battaglia et al. 2000b) fold increase in height has been documented. A major cause of this increase is related to the intensified burning rate (Chuah and Kushida 2007), due to increased heat transfer at the fuel surface, and circulation, which modifies entrainment and mixing. The flame height has been found to increase with applied circulation, even when the burning rate and the fuel source diameter (D_0) are constant (Chigier et al. 1970; Battaglia et al. 2000a). In order to describe this behavior, Kuwana et al. (2008) utilized scaling analysis to describe this relationship,

$$\frac{H}{D_0} \sim \begin{cases} \left(\dfrac{\Gamma^2}{gD_0^3}\right)^{1/3} & \text{for} \quad \dfrac{\Gamma^2}{gD_0^3} \to \infty \\ \left(\dfrac{\Gamma^2}{gD_0^3}\right) & \text{for} \quad \dfrac{\Gamma^2}{gD_0^3} \to 0 \end{cases} \tag{5.1}$$

In equation 5.1, very large values of $\Gamma^2/(gD_0^3)$ correspond to small pool fires while very small values correspond to large pool fires. The result of equation 5.1 asymptotically converges to simulation results of Battaglia et al. (2000b) as $\Gamma^2/(gD_0^3)$ increases. This suggests that, for small fire whirls, the flame height is circulation-controlled, whereas for large fire whirls other parameters such as the burning rate and buoyancy are also dominant. Chow et al. (2010) also established a positive correlation between the fire whirl height and the product of the dimensionless fire power, $\dot{\mathcal{Q}}^*$, and pool diameter, as $H = 3.59\dot{\mathcal{Q}}^{*2/5}D_0$.

It has been argued that the flame radius in the continuous flame region is nearly equal to that of the vortex core above the radial boundary layer (Byram and Martin 1962; Lei et al. 2011). Given this and assuming that the flame has a quasi-steady axisymmetric state with constant ambient circulation in the axial direction that follows the Burgers vortex model, a power-law relation is obtained as $b_w \sim (HD_0^\eta)/\Gamma$, where η is a fitting exponent. The inverse relationship of b_w with circulation is in agreement with the results

of Battaglia et al. (2000b)'s inviscid model. Considering discussions on the turbulence suppression mechanism (see section 5.3), and following the scaling expression for vortex core radius, one can infer that the fire whirl height is a function of both burning rate and circulation. This is evident in results of dimensional analysis as $H = \mathcal{G} D_0 (\dot{\mathcal{Q}}^* \Gamma^{*2})^{\eta_m}$ in which $\dot{\mathcal{Q}}^*$ is the dimensionless fire power (see section 2), $\Gamma^* = \Gamma/\sqrt{gD_0^3}$, and η_m as well as $\mathcal{G}$ are empirically-obtained variables (Lei et al. 2011). These results agree with measurements by Emmons and Ying (1967). Based on these results, a flame height expression can be obtained as $H = \Gamma^{*\eta_S(2+\eta_m)} D_0^{1+3\eta_S(\eta_m-1)/2}$, where for laminar fire whirls η_m and η_S are 0.5 and 0.4, respectively (Lei et al. 2012). For turbulent boundary layers at the base, these values change to 1 and 1/3, respectively. The results are consistent with observations of Emori and Saito (1982) for laminar fire whirls and appear to hold true prior to the formation of any vortex breakdown. Zhou et al. (2013) also proposes that, if one normalizes the fire whirl's flame height with the flame height of a similar non-swirling fire, there is a linear correlation in the logarithmic space between the normalized heights and circulation. Further, based on PIV measurement results, Hartl and Smits (2016) proposed a scaling relationship, i.e $H = 0.7 D_0 \Gamma^{*1.11}$, which implies that circulation is the dominant parameter in determining a fire whirl's height. These results appear to provide a better fit to the experimental data than the correlation proposed by Kuwana et al. (2008).

5.2. Boundary Layer & Burning Rate

As mentioned previously, the presence of drag (friction) at the base is crucial for fire whirl formation. Previous studies by Morton (1970), Emmons and Ying (1967), and Dobashi et al. (2015) suggest that disruption of the cyclostropic balance at the base and formation of an Ekman-type inflow boundary layer due to viscous effects, change the flame shape such that the heat and mass transfer rates on the fuel surface, i.e. the burning rate, increase significantly in relation to non-whirling fires or whirling flames without viscous effects at their base; see figure 8-(right). This is consistent with the Ekman-layer solution on a solid surface where the balance between circulation, pressure gradient, and friction (drag) force withing the boundary layer delivers velocity component towards the low pressure zone, i.e. radial inflow (Kundu et al. 2008). In fire whirls, the behavior of the boundary layer, circulation, and burning rate are all interrelated. In this regard, in a set of pool fire whirl experiments, Lei et al. (2012) observed that the fuel surface often oscillates slightly due to flame wander and the presence of unstable secondary flows. In relatively large fire whirls, circular ripples are continuously generated and move towards the center of the liquid fuel surface, due to the strong inflow at the boundary layer. Also, as the height of ripples increases, these wave-like structures approach the center. In rare cases, with relatively strong circulation, the ripples were reported to abruptly break into sprays in the center and evaporate through the high temperature core (Lei et al. 2012). Under strong circulation it is found that liquid fuel can be directly sucked into the vortex core and, in the case of solid combustible materials, this may lead to a firebrand shower and subsequent spot fire ignitions as solid fuels have much slower pyrolysis rates than liquid fuels. With regard to these observations, Lei et al. (2012) concludes that although dynamics of these complex interactions is not fully understood, collectively, they may enhance the fuel evaporation rate.

Previous studies have reported a dramatic increase in the burning rate provided by the fire whirl, 1.4 - 4.2 times the original burning rate of a non-whirling fire, for wildland (solid)

fuels (Martin et al. 1976). Emmons and Ying (1967)'s pioneering study with an acetone pool fire whirl also showed that the mass-loss rate increases monotonically with increasing ambient circulation. Following the discussion above, heat transfer at the fuel surface was thought to increase significantly due to the flow structure (presence of swirl), effectively increasing the heat transfer coefficient for fire whirls (Muraszew et al. 1979). In larger fire sizes, the radiative heat feedback fraction was found to increase for fire whirls as opposed to the corresponding pool fires (Zhou et al. 2011). However Snegirev et al. (2004) found that this fraction decreases, slightly, with circulation. This indicates that the increase in burning rate is still due to enhanced air entrainment through the Ekman-type boundary layer adjacent to the fuel surface.

Interestingly, the diameter of the vortex core (D_w) was found to increase inversely with the diameter of the fuel surface (Chuah et al. 2009). Following this observation, Lei et al. (2012) argued that the inflow boundary layer can be separated into an inner non-reactive, $r \leq R_{I.N.}$, and an outer reactive, $R_{I.N.} < r \leq R_{O.R.}$, regions as shown in figure 8-(left). The mechanisms of heat and mass transfer within these regions are considerably

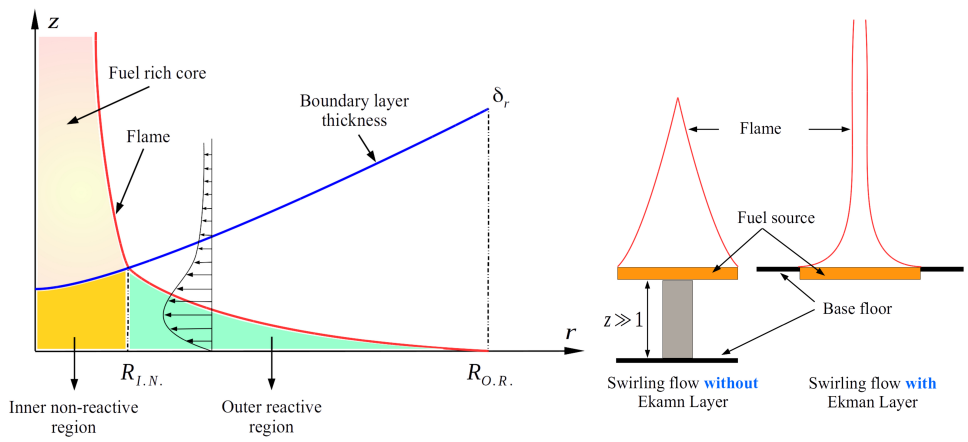

Figure 8

(left) Schematic showing the different regions within the boundary layer at the base of a fire whirl following Lei et al. (2012) and (right) viscous effects of the Ekman boundary layer on the flame shape at the base of a fire whirl following Dobashi et al. (2015)

.

different. It is experimentally shown that viscous effects near the surface, i.e. the Ekman layer, cause the flame base to approach the fuel surface, increasing heat transfer and the burning rate (Dobashi et al. 2015). Given this, estimation of the burning rate in a laminar boundary layer will be different than a turbulent one. For turbulent boundary layers with $Pr \approx 1$, convective heat transfer on the fuel surface can be related to the wall friction by extension of the Chilton-Colburn analogy (Bergman et al. 2011; Rotta 1964). In fire whirls with laminar boundary layers, the Chilton-Colburn analogy is not appropriate, since a large radial pressure gradient exists. However, Glassman et al. (2014) showed that, for a laminar convective burning problem, the mass-loss rate per unit area can be approximated by stagnant film theory, using a radiation correction from Fineman (1962). Given these, integration of the momentum equations for turbulent and laminar boundary layers results in the total mass-loss rate ($\dot{m}$) in fire whirls as $\dot{m} = \mathcal{G}\Gamma^{1/(\eta_m+1)}R_{O.R.}$, where $\mathcal{G}$ is a function

of various parameters including the entrainment coefficient (Lei et al. 2012). For laminar boundary layers $\eta_m = 1$, while for turbulent cases η_m depends on the surface roughness which varies between $1/7 - 1/4$. Results of these semi-empirical expressions compare well with the experimental data of Emmons and Ying (1967) and Lei et al. (2012).

5.3. Vortex Breakdown, Turbulence Suppression & Entrainment

The flow structure of a quasi-steady on-source fire whirl is, primarily, formed and sustained by its unique entrainment mechanism, which in turn can be affected by phenomena such as vortex breakdown and turbulence suppression. In Emmons and Ying (1967)'s theory, the mixing coefficient decreases with increasing circulation strength. This suppresses molecular entrainment of oxygen from the ambient to the vortex core and results in flame elongation. It is observed that the spiral rise of fluid in the core is surrounded by a rapidly rotating free vortex which generates surface waves on the core which move with $U_{wave} = \Gamma/(4\pi b_w)$ (Emmons and Ying 1967). Analogous to a hydraulic jump, if the fire whirl core travels faster or slower than U_{wave}, it corresponds respectively to shooting or tranquil flow. This, particularly, is the case once vortex breakdown occurs. It is important that turbulent suppression damps the effective entrainment of air into the vortex core through the part that is from above the boundary layer up to the intermittent flame zone (Lei et al. 2015b). However, the presence of vortex breakdown, which is accompanied with high turbulence and circulation, accounts for highly effective entrainment in the plume region as well as growth of b_w beyond the intermittent flame zone. High circulation, which may lead to vortex breakdown, increases the inflow rate and subsequently the entrainment through the boundary layer thickness (Zhou et al. 2013). Experimental results of Zhou et al. (2013) suggest that air entrained through the boundary layer is sufficient for sustained complete combustion. Also, it is found that, above the boundary layer thickness and through the flaming region, the (dimensionless) mass-flow rate gradually rises and drastically increases in the vertical direction. Eventually, the mass-flow rate decays in the plume region. Hence, several entrainment zones can be identified along the fire whirl height (Zhou et al. 2013). In experiments of Lei et al. (2015b), variations in mass flow rate with height show that the entrained air through the inflow boundary layer is often not sufficient for stoichiometric combustion of the fuel, even though the air and fuel are relatively well-mixed. Nonetheless, consistent with Zhou et al. (2013), $\dot{m}$ varies, considerably through the height. As a result, fire whirls consist of a laminarized zone at lower height which coexist with turbulent regions at increasing heights. This notion justifies highly suppressed entrainment within the continuous flame region and appreciable mixing through the plume region (Zhou et al. 2013; Lei et al. 2015b).

A considerable reduction in mixing and entrainment along swirling jet flames, due to turbulence suppression, has been documented by Chigier et al. (1970). In quasi-steady on-source fire whirls, where the flame core radius is relatively steady, mixing is quite different than pool fires, where this radius varies significantly as a function of time due to intermittent "puffing" of the flame (Tieszen 2001). Therefore, the flow field of a fire whirl can be described as an inner fuel-rich jet within a coaxial stream with swirl, through which the entrained air mixes with the fuel gradually in the flaming region (Lei et al. 2015b). As a result, two turbulent suppression mechanisms are identified in order to describe such behavior. The first mechanism is due to a radial force balance, where the radially-outward centrifugal force is equal to the radially inward pressure gradient ($\partial p/\partial r \sim \rho U_\theta^2/r$). This

so-called cyclostropic balance, which suppresses the transverse motion of fluid particles in the radial direction, leads to a reduction in turbulent mixing along the vortex core height. From a different perspective, others (Beér and Chigier 1972) attribute the suppression in mixing to a reduction of shear stresses at the vortex-core interface. Regardless of the cause, this mechanism can be quantified by introducing a simple Richardson number as $Ri_A \sim (U_{\theta,max}/U_{z,max})^2$ (Lei et al. 2015b). The proposed Richardson number is analogous to the swirl number which is used to characterize the circulation strength in swirling jets (Ellison and Turner 1959). The larger the value of Ri_A, the more intense the turbulence suppression will become.

The second mechanism results from stable stratification in the radial direction (Lei et al. 2015b). In fact, the density gradient and the centrifugal acceleration are both radially outward (Ellison and Turner 1959). Hence, contrary to the role of buoyancy in increasing mixing through the gravity field, this stable stratification reduces turbulent fluctuations and subsequently mixing at the vortex core interface in the r direction. These effects can be quantified by $Ri_B = (\Delta\rho_m/\rho_\infty)(U_{\theta,max}/U_{z,max})^2$ (Lei et al. 2015b). The greater the value of Ri_B, the more the turbulent mixing is suppressed. Further, Lei et al. (2015b) shows that the entrainment coefficient (α) and Ri_B are inversely proportional. This is comparable to the turbulent mixing regime, due to the coexistence of intermittent vortex mixing and continuous entrainment along the cusp of the fire whirl core (Christodoulou 1986).

5.3.1. The Blue Whirl. Recent experiments have revealed an exciting new phenomenon described as the "blue whirl". Using a conventional fire whirl setup similar to figure 4-(a), Xiao et al. (2016) observed a traditional fire whirl which underwent what is thought to be a bubble-mode of vortex breakdown. The major modification between this setup and previous experiments was that it was formed over a water surface which provided a smoother boundary and emphasized the effects of the radial boundary layer on the flame structure. The resulting flame shown in figure 1-(d) consists of a light blue cone at the base, a bright ring, and a purple haze above.

One of the most fascinating aspects of this flame is that, once transitioned, it burned without any yellow flame, indicating soot-free combustion, even when directly burning n-heptane, which is usually a sooty fuel. Two physical mechanisms were speculated to be important for the formation of a blue whirl, vortex breakdown and fast mixing. As a yellow fire whirl is formed, it was seen to transition to what resembles a bubble-mode vortex breakdown with a stagnation point and recirculation zone at the core of the vortex. During the transition, this could be visualized with soot remaining from a yellow whirl entraining into the recirculation zone of the blue whirl. Fast mixing rates are expected that may favor soot-free combustion, similar to effects seen in highly strained co-flow or opposed-jet diffusion flames (Lin and Faeth 1996a,b).

Many questions still remain as to the source of and processes occurring during transition and steady burning of a blue whirl. For instance, measurements or simulations of the flow field during the transition process or steady burning have not yet been completed, so a complete understanding of the fluid dynamic processes occuring is not yet here.

6. CONCLUSIONS AND FUTURE DIRECTIONS

Despite many years of study, the fire whirl still continues to fascinate the scientific community and present challenges for fire safety. Without a definitive theory of the flow structure

for a fire whirl, many gaps remain in our understanding. Much progress has been made with regard to on-source, quasi-steady fire whirls, such as those formed in enclosed laboratory apparatus. However, some open questions remain. First and foremost the underlying process governing entrainment does not seem to be well known. Starting from Emmons and Ying (1967) early work, clear issues were raised with regard to the treatment of entrainment as a function of height, and it seems these have yet to be resolved. Some detailed PIV measurements have assisted in this understanding, but it is still not fully resolved. This will help us better formulate a model of the fire whirl.

Other types of fire whirls, in particular those that occur off-source and those that are non-steady, continue to challenge our understanding. Certainly the velocity and temperature fields within these whirls may differ, but exactly how remains to be seen. A reliable method of generating these whirls within the laboratory and detailed measurements of the structure would be very beneficial to this understanding. Even stationary fire whirls over a fuel source precess around that source, causing them to move and "wander," causing unknown effects to the structure of the fire whirl, especially when they are near their limits of stability (e.g. fuel-rich or high swirl). The effects of the level of circulation (e.g. Rossby number) on the structure of fire whirls is not well-known as most experiments have been performed only under a limited range of circulation and scale.

Scaling laws describing the formation of these complex whirls have begun and highlight their dependence on ambient cross-flow, however there is no general form which describes the conditions for generation of a fire whirl. This knowledge would certainly be useful in operational modeling of wildfires, where resolutions are too coarse to resolve complicated flow dynamics leading to fire whirls, but predictions of critical conditions conditions could be used to send a warning to firefighters that might be in danger of being present near fire whirl formation.

The use of numerical modeling has been relatively lacking in this field compared to many other areas of fluid dynamics, combustion and fire phenomenon. This may be due to the complex interactions that occur during the generation and growth of a fire whirl, however numerical models could provide invaluable information if validated against experimental measurements. Continued development of these models, particularly for cases other than stationary, on-source fire whirls, is highly encouraged. This may also be useful in understanding the formation of fire whirls, especially under wind, visualizing flow structures that cannot be easily measured experimentally.

The prospect of "efficient" combustion, highlighted by discovery of the blue whirl, also presents many opportunities for fire whirl research. If fuel spills could be removed with significantly reduced emissions (e.g. minimal soot) it may be much easier to alleviate the hazardous consequences of oil spills. Even if blue whirls cannot be formed at this scale, traditional fire whirls produce higher mass-loss rates of fuel, burn at higher temperatures, and have been observed to entrain liquid fuel at their center, which may all be favorable for fuel spill remediation. Energy production in unique environments may also benefit from this efficient configuration, though precise control of the process will be vital to its practical implementation. Scientifically, the blue whirl and its transition from fire whirls may present an interesting platform to learn about the formation of soot from different fuel sources and the phenomenon of vortex breakdown.

DISCLOSURE STATEMENT

The authors are not aware of any affiliations, memberships, funding, or financial holdings that might be perceived as affecting the objectivity of this review.

ACKNOWLEDGMENTS

The authors gratefully acknowledge Sriram Bharath Hariharan for performing experiments displayed in several figures and both he and Ajay Vikram Singh for their contributions to our understanding of the blue whirl. The authors would also like to thank Forman Williams, Antonio Sanchez, Alexander Smits, Katie Hartl, and Elaine Oran for interesting discussions which improved this manuscript. Support for this work came from the National Science Foundation under awards CBET-1507623 and CBET-1554026 and the USDA Forest Service Missoula Fire Sciences Laboratory, National Fire Decision Support Center under collaborative agreement 13-CS-11221637-124. Any opinions, findings, and conclusions or recommendations expressed in this material are those of the author(s) and do not necessarily reflect the views of the National Science Foundation or USDA Forest Service.

LITERATURE CITED

Akhmetov, D. G., Gavrilov, N. V., and Nikulin, V. V. (2007). Flow structure in a fire tornado-like vortex. *Doklady Physics*, 52(11):592–595.

Albini, F. A. (1984). Wildland fires: Predicting the behavior of wildland fires among nature's most potent forces-can save lives, money, and natural resources. *American Scientist*, 72(6):590–597.

Batchelor, G. (1953). *The Theory of Homogeneous Turbulence*. Cambridge University Press, Cambridge, London, England.

Batchelor, G. K. (2000). *An introduction to fluid dynamics*. Cambridge University Press, Cambridge, London, England.

Battaglia, F., McGrattan, K. B., Rehm, R. G., and Baum, H. R. (2000a). Simulating fire whirls. *Combustion Theory and Modelling*, 4(2):123–138.

Battaglia, F., Rehm, R. G., and Baum, H. R. (2000b). The fluid mechanics of fire whirls: An inviscid model. *Physics of Fluids*, 12(11):2859–2867.

Beér, J. M. and Chigier, N. A. (1972). Combustion aerodynamics. *Applied Science Publication*.

Bergman, T., Incropera, F., DeWitt, D., and Lavine, A. (2011). *Fundamentals of heat and mass transfer*. Wiley, New Jersey.

Bödewadt, U. (1940). Die drehströmung über festem grunde. *ZAMM-Journal of Applied Mathematics and Mechanics/Zeitschrift für Angewandte Mathematik und Mechanik*, 20(5):241–253.

Burgers, J. M. (1948). A mathematical model illustrating the theory of turbulence. *Advances in applied mechanics*, 1:171–199.

Byram, G. and Martin, R. (1962). Fire whirlwinds in the laboratory. *Fire Control Notes*, 23(1):13–17.

Byram, G. M. and Martin, R. E. (1970). The Modeling of Fire Whirlwinds. *Forest Science*, 16:386–399.

Chigier, N., Beer, J., Grecov, D., and Bassindale, K. (1970). Jet flames in rotating flow fields. *Combustion and Flame*, 14(2):171–179.

Chow, W. K., He, Z., and Gao, Y. (2010). Internal Fire Whirls in a Vertical Shaft. *Journal of Fire Sciences*, 29(1):71–92.

Christodoulou, G. (1986). Interfacial mixing in stratified flows. *Journal of hydraulic research*, 24(2):77–92.

Chuah, K. H. and Kushida, G. (2007). The prediction of flame heights and flame shapes of small fire whirls. *Proceedings of the Combustion Institute*, 31 II:2599–2606.

Chuah, K. H., Kuwana, K., and Saito, K. (2009). Modeling a fire whirl generated over a 5-cm-diameter methanol pool fire. *Combustion and Flame*, 156(9):1828–1833.

Chuah, K. H., Kuwana, K., Saito, K., and Williams, F. A. (2011). Inclined fire whirls. *Proceedings of the Combustion Institute*, 33(2):2417–2424.

Church, C. R., Snow, J. T., and Dessens, J. (1980). Intense atmospheric vortices associated with a 1000 mw fire. *Bulletin of the American Meteorological Society*, 61(7):682–694.

Countryman, C. M. (1971). Fire whirls, why, when, and where.

Dessens, J. (1962). Man-made Tornadoes. *NATURE*, 193(4810):13.

Dobashi, R., Okura, T., Nagaoka, R., Hayashi, Y., and Mogi, T. (2015). Experimental study on flame height and radiant heat of fire whirls. *Fire Technology*, 52(4):1069–1080.

Donaltson, C. d. P., Sullivan, R., et al. (1960). Behavior of solutions of the navier–stokes equations for a complete class of three-dimensional viscous vorticies. In *Proc. Heat Transfer Fluid Mech. Inst.*, pages 16–30.

Ellison, T. and Turner, J. (1959). Turbulent entrainment in stratified flows. *Journal of Fluid Mechanics*, 6(03):423–448.

Emmons, H. W. and Ying, S.-J. (1967). The fire whirl. *Proceedings of the Combustion Institute*, 11(1):475–488.

Emori, R. I. and Saito, K. (1982). Model experiment of hazardous forest fire whirl. *Fire Technology*, 18(4):319–327.

Fineman, S. J. (1962). Some analytical considerations of the hybrid rocket combustion problem.

Forthofer, J. M. and Goodrick, S. L. (2011). Review of vortices in wildland fire. *Journal of Combustion*, 2011:1–14.

Glassman, I., Yetter, R., and Glumac, N. (2014). *Combustion*. Elsevier Science, Amsterdam, Netherlands.

Grishin, A. (2007). Effect of the interaction between fire tornadoes on their propagation. In *Doklady Physics*, volume 52, pages 521–522.

Grishin, A., Golovanov, A., Kolesnikov, A., Strokatov, A., and Tsvyk, R. S. (2005). Experimental study of thermal and fire tornadoes. In *Doklady Physics*, volume 50, pages 66–68.

Hamins, A., Kashiwagi, T., and Buch, R. R. (1996). Characteristics of pool fire burning. In *Fire Resistance of Industrial Fluids, STP16278S*. ASTM International, West Conshohocken, PA, USA.

Hartl, K. A. (2016). Experimental investigation of laboratory fire whirls.

Hartl, K. A. and Smits, A. J. (2016). Scaling of a small scale burner fire whirl. *Combustion and Flame*, 163:202–208.

Hassan, M. I., Kuwana, K., Saito, K., and Wang, F. (2005). Flow structure of a fixed-frame type fire whirl. *Fire Safety Science*, 8:951–962.

Hayashi, Y., Kuwana, K., and Dobashi, R. (2011). Influence of vortex structure on fire whirl behavior. *Fire Safety Science*, 10:671–679.

Hunt, G. and Kaye, N. G. (2001). Virtual origin correction for lazy turbulent plumes. *Journal of Fluid Mechanics*, 435:377–396.

Klimenko, A. (2014). Strong swirl approximation and intensive vortices in the atmosphere. *Journal of Fluid Mechanics*, 738:268–298.

Klimenko, A. and Williams, F. (2013). On the flame length in firewhirls with strong vorticity. *Combustion and Flame*, 160(2):335–339.

Kundu, P., Cohen, I., and Hu, H. (2008). Fluid mechanics. 2004. *Elsevier Academic Press, San Diego).*, 307:471–476.

Kuwana, K., Morishita, S., Dobashi, R., Chuah, K. H., and Saito, K. (2011). The burning rate's effect on the flame length of weak fire whirls. *Proceedings of the Combustion Institute*, 33(2):2425–2432.

Kuwana, K., Sekimoto, K., Minami, T., Tashiro, T., and Saito, K. (2013). Scale-model experiments of moving fire whirl over a line fire. *Proceedings of the Combustion Institute*, 34(2):2625–2631.

Kuwana, K., Sekimoto, K., Saito, K., and Williams, F. (2008). Scaling fire whirls. *Fire Safety Journal*, 43(4):252–257.

Kuwana, K., Sekimoto, K., Saito, K., Williams, F. A., Hayashi, Y., and Masuda, H. (2007). Can we predict the occurrence of extreme fire whirls? *AIAA journal*, 45(1):16–19.

Lee, J. H.-w. and Chu, V. (2012). *Turbulent jets and plumes: a Lagrangian approach*. Springer Science & Business Media, New York, USA.

Lee, S.-L. and Garris, C. A. (1969). Formation of multiple fire whirls. In *Proceedings of the Combustion Institute*, volume 12, pages 265–273.

Lei, J. and Liu, N. (2016). Flame precession of fire whirls: A further experimental study. *Fire Safety Journal*, 79:1–9.

Lei, J., Liu, N., Lozano, J. S., Zhang, L., Deng, Z., and Satoh, K. (2013). Experimental research on flame revolution and precession of fire whirls. *Proceedings of the Combustion Institute*, 34(2):2607–2615.

Lei, J., Liu, N., and Satoh, K. (2015a). Buoyant pool fires under imposed circulations before the formation of fire whirls. *Proceedings of the Combustion Institute*, 35(3):2503–2510.

Lei, J., Liu, N., Zhang, L., Chen, H., Shu, L., Chen, P., Deng, Z., Zhu, J., Satoh, K., and De Ris, J. L. (2011). Experimental research on combustion dynamics of medium-scale fire whirl. *Proceedings of the Combustion Institute*, 33(2):2407–2415.

Lei, J., Liu, N., Zhang, L., Deng, Z., Akafuah, N. K., Li, T., Saito, K., and Satoh, K. (2012). Burning rates of liquid fuels in fire whirls. *Combustion and Flame*, 159(6):2104–2114.

Lei, J., Liu, N., Zhang, L., and Satoh, K. (2015b). Temperature, velocity and air entrainment of fire whirl plume: A comprehensive experimental investigation. *Combustion and Flame*, 162(3):745–758.

Lin, K.-C. and Faeth, G. (1996a). Hydrodynamic suppression of soot emissions in laminar diffusion flames. *Journal of Propulsion and Power*, 12(1):10–17.

Lin, K.-C. and Faeth, G.-M. (1996b). Effects of hydrodynamics on soot formation in laminar opposed-jet diffusion flames. *Journal of propulsion and power*, 12(4):691–698.

Liu, N., Liu, Q., Deng, Z., Kohyu, S., and Zhu, J. (2007). Burn-out time data analysis on interaction effects among multiple fires in fire arrays. *Proceedings of the Combustion Institute*, 31(2):2589–2597.

Martin, R. E., Pendleton, D. W., and Burgess, W. (1976). Effect of fire whirlwind formation on solid fuel burning rates. *Fire Technology*, 12(1):33–40.

Matsuyama, K., Tanaka, F., Ishikawa, N., Tanaka, S., Ohmiya, Y., and Hayashi, Y. (2004). Experimental and numerical studies on fire whirls. *Fire Safety Science*, 6:2–13.

McCaffrey, B. J. (1979). Purely buoyant diffusion flames: some experimental results. *NBSIR*, pages 79–1910.

McRae, R. H., Sharples, J. J., Wilkes, S. R., and Walker, A. (2013). An australian pyrotornadogenesis event. *Natural hazards*, 65(3):1801–1811.

Morton, B. (1970). The physics of fire whirls. In *Fire Research Abstracts and Reviews*, volume 12, pages 1–19.

Morton, B., Taylor, G., and Turner, J. (1956). Turbulent gravitational convection from maintained and instantaneous sources. In *Proceedings of the Royal Society of London A: Mathematical, Physical and Engineering Sciences*, volume 234, pages 1–23. The Royal Society.

Mullen, J. B. and Maxworthy, T. (1977). A laboratory model of dust devil vortices. *Dynamics of Atmospheres and Oceans*, 1(3):181–214.

Muraszew, A., Fedele, J., and Kuby, W. (1979). The fire whirl phenomenon. *Combustion and Flame*, 34:29–45.

Nydahl, J. E. (1971). Heat transfer for the bödewadt problem.

Quintiere, J. (2006). *Fundamentals of fire phenomena*. Wiley, New Jersey.

Rotta, J. (1964). Temperaturverteilungen in der turbulenten grenzschicht an der ebenen platte. *International Journal of Heat and Mass Transfer*, 7(2):215–228.

Satoh, K. and Yang, K. (2000). A horizontal fire-whirl design scenario for engineering performance-based fire-code applications. *Int. Journal on Engineering Performance-Based Fire Codes*, 2(2):48–57.

Satoh, K. and Yang, K.-T. (1996). Experimental observations of swirling fires. *ASME-PUBLICATIONS-HTD*, 335:393–400.

Satoh, K., Yang, K. T., and Dame, N. (1997). Simulations of Swirling Fires Controlled by Channeled Self-generated Entrainment Flows. *Fire Safety Science*, 5:201–212.

Sharples, J. J., Kiss, A. E., Raposo, J., Viegas, D. X., and Simpson, C. C. (2015). Pyrogenic vorticity from windward and lee slope fires. In 21st *International Congress on Modeling and Simulation*, pages 291–297.

Simpson, C., Sharples, J. J., Evans, J. P., et al. (2016). Sensitivity of atypical lateral fire spread to wind and slope. *Geophysical Research Letters*, 43:1744–1751.

Smits, A., Hartl, K., Guo, S., and Dryer, F. (2012). Laboratory Studies of Fire Whirls.

Snegirev, A., Marsden, J., Francis, J., and Makhviladze, G. (2004). Numerical studies and experimental observations of whirling flames. *International Journal of Heat and Mass Transfer*, 47(12-13):2523–2539.

Soma, S. and Saito, K. (1988). A study of fire whirl on mass fires using scaling models. In *Proceedings of the First International Symposium on Scale Modeling*, page 353. The Japan Society of Mechanical Engineers.

Soma, S. and Saito, K. (1991). Reconstruction of fire whirls using scale models. *Combustion and Flame*, 86(3):269–284.

Stewartson, K. (1953). On the flow between two rotating coaxial disks. In *Mathematical Proceedings of the Cambridge Philosophical Society*, volume 49, pages 333–341. Cambridge Univ Press.

Thomas, P. (1963). The size of flames from natural fires. In *Proceedings of the Combustion Institute*, volume 9, pages 844–859. Elsevier.

Tieszen, S. R. (2001). On the fluid mechanics of fires 1. *Annual review of fluid mechanics*, 33(1):67–92.

Tohidi, A. and Kaye, N. B. (2016). Highly buoyant bent-over plumes in a boundary layer. *Atmospheric Environment*, 131:97–114.

Turner, J. S. (1979). *Buoyancy effects in fluids*. Cambridge University Press, Cambridge, London, England.

Wang, P., Liu, N., Hartl, K., and Smits, A. (2016). Measurement of the Flow Field of Fire Whirl. *Fire Technology*, 52(1):263–272.

Wang, P., Liu, N., Zhang, L., Bai, Y., and Satoh, K. (2015). Fire Whirl Experimental Facility with No Enclosure of Solid Walls: Design and Validation. *Fire Technology*, 51(4):951–969.

Xiao, H., Gollner, M. J., and Oran, E. S. (2016). From fire whirls to blue whirls and combustion with reduced pollution. *Proceedings of the National Academy of Sciences*, 113(34):9457–9462.

Ying, S. J. and Chang, C. (1970). Exploratory model study of tornado-like vortex dynamics. *Journal of the Atmospheric Sciences*, 27(1):3–14.

Zhou, K., Liu, N., Lozano, J. S., Shan, Y., Yao, B., and Satoh, K. (2013). Effect of flow circulation on combustion dynamics of fire whirl. *Proceedings of the Combustion Institute*, 34(2):2617–2624.

Zhou, K., Liu, N., and Satoh, K. (2011). Experimental research on burning rate, vertical velocity and radiation of medium-scale fire whirls. *Fire Safety Science*, 10:681–691.

Zhou, K., Liu, N., and Yuan, X. (2016). Effect of wind on fire whirl over a line fire. *Fire Technology*, 52(3):865–875.

Zhou, K., Liu, N., Zhang, L., and Satoh, K. (2014). Thermal Radiation from Fire Whirls: Revised Solid Flame Model. *Fire Technology*, 50(6):1573–1587.

Zhou, R. and Wu, Z.-N. (2007). Fire whirls due to surrounding flame sources and the influence of the rotation speed on the flame height. *Journal of Fluid Mechanics*, 583:313–345.